

TURBULENT DIFFUSION OF SCALAR AND HEAT IN AN OFF-SOURCE HEATED STEADY ROUND JET

Rohit Singhal

Department of Aerospace Engineering
Indian Institute of Science
Bengaluru, Karnataka-560012, India
rohitsinghal@iisc.ac.in

S. Ravichandran

Nordic Institute for Theoretical Physics
KTH Royal Institute of Technology
and Stockholm University
Stockholm, SE-106 91, Sweden
ravichandran@su.se

Sourabh S. Diwan

Department of Aerospace Engineering
Indian Institute of Science
Bengaluru, Karnataka-560012, India
sdiwan@iisc.ac.in

ABSTRACT

We study, using direct numerical simulation (DNS), the properties of a steady jet heated externally in a heat-injection zone, the rate of heat addition being proportional to the local concentration of a scalar. We examine the turbulent diffusivities of the scalar concentration, the temperature and the axial momentum, and compare their values with those for unheated jets and plumes. We also include results from the available literature and compare them with our results where possible. We find that external heat addition decreases the turbulent scalar diffusivity, leading to a decrease in the ratio of scalar to velocity flow widths relative to the unheated jet to a value that is largely insensitive to the precise details of heat addition, except for one study. We also find that while the turbulent thermal diffusivity also decreases, the ratio of temperature to velocity flow widths is similar to those for unheated plumes. Our results suggest that further studies of off-source heated jets are warranted.

INTRODUCTION

Cumulus clouds play a key role in the transport of heat and water vapour in the Earth's atmosphere. Yet, the current understanding of cumulus convection, and in particular the dynamics of entrainment, remains incomplete. The release of latent heat by the condensation of water vapour in cumulus clouds makes them qualitatively different from jets and plumes (e.g. Narasimha *et al.*, 2011). Previous studies have examined the role of such 'off-source' heat addition in modifying the dynamics of plumes (e.g. Venkatakrishnan, 1997) and jets (e.g. Bhat & Narasimha, 1996), finding that external heating fundamentally alters the dilution and diffusion characteristics of the flow. Previous experimental, direct numerical simulation (DNS) and Large eddy simulation (LES) studies of steady jet with off-source heat addition are listed in Table 1.

These studies, and in particular that of Bhat & Narasimha (1996), attempted to characterise the anomalous entrainment in externally heated flows, and hence focused on the turbulent diffusion of momentum. They also found that the scalar distribution attains a Gaussian radial profile even with external

Table 1. Experimental (Exp) and numerical (DNS/LES) studies of off-source heated jet with their respective locations of heat injection zone (z_b-z_t) and heating numbers G (see text for definition).

Study	Type	z_b-z_t	G
Present	DNS	15d-35d	0.37
Bhat & Narasimha (1996)	Exp	133d-213d	0.007-0.16
Venkatakrishnan (1997)	Exp	53d-83d	0.06
Agrawal & Prasad (2004)	Exp	200d-265d	0.2
Agrawal <i>et al.</i> (2005)	DNS	23d-31d	12
Aspden <i>et al.</i> (2017)	LES	10d-14d	0.075-0.8
Kewalramani <i>et al.</i> (2022)	LES	30d-42d	0.075-0.8

heat addition (as is the case with velocity distribution), and that the growth rate of the scalar-profile width reduces upon heat addition. The scalar concentration here is analogous to the water vapour concentration in clouds, which controls the rate of condensation-heating.

In this study, we aim to better understand the diffusion of the scalar concentration and temperature in externally heated jets. To this end, we perform DNS of an off-source heated jet and find, in agreement with earlier observations, that the ratio of scalar- to velocity-profile widths reduces upon heat addition. We find, interestingly, that this ratio falls in a narrow range beyond the heating zone for most of the reported cases, largely independent of the details of heat addition. Our results show that the turbulent diffusivity of the scalar (defined below) decreases upon heat addition, leading to a greater turbulent Schmidt number, especially within the core of the heated jet. The turbulent Prandtl number also increases in the core, but is associated with a qualitatively different radial profile of temperature with peaks away from the jet axis. Lastly, we show that the acceleration of the flow by off-source heat addition results in the total scalar content (scalar concentration integrated over the horizontal plane) remaining nearly constant with axial distance.

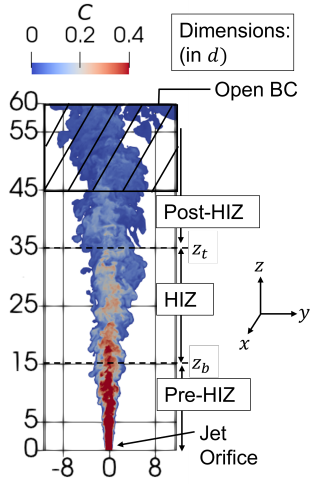


Figure 1. A contour plot showing the passive scalar concentration on a vertical plane through the centerline of an off-source heated jet. Heat is added to the flow in the region $z_b = 15d < z < z_t = 35d$.

NUMERICAL SIMULATION DETAILS

The governing equations are the Boussinesq-Navier-Stokes equations, coupled with transport equations for the temperature and the scalar concentration through the buoyancy term, as described in Aspden *et al.* (2017),

$$\begin{aligned} \nabla \cdot \mathbf{u} &= 0, \quad D\mathbf{u}/Dt = -\nabla p + (1/Re)\nabla^2 \mathbf{u} + (g\beta_T d/U_o^2)Te_z, \\ DT/Dt &= [1/(Re \cdot Pr)]\nabla^2 T + (\alpha_C d/U_o)\mathcal{H}C, \\ DC/Dt &= [1/(Re \cdot Sc)]\nabla^2 C. \end{aligned} \quad (1)$$

These equations have been nondimensionalised using the orifice diameter (d), the orifice velocity (U_o) and orifice scalar concentration (C_o) as the scales. The non-dimensional temperature (T) at the orifice is chosen to be zero, and only becomes non-zero when the flow is externally heated; the flow is thus entirely momentum-driven at the orifice. The source term $(\alpha_C d/U_o)\mathcal{H}C$, where C represent scalar concentration field and α_C is the maximum heating rate, controls the rate of heat addition. The Heaviside function $\mathcal{H} = 1$ in the heat injection zone (HIZ, $z_b = 15d < z < z_t = 35d$ in the present study), and vanishes elsewhere (see figure 1(a)). The scalar concentration which controls the rate of heating and thus the buoyancy $g\beta_T d/U_o^2$ of the flow, where g is gravitational acceleration and β_T is thermal expansion coefficient, is itself advected by the flow. This coupling is responsible for the intricacy of the resulting dynamics.

The flow is governed by the nondimensional Reynolds number $Re = 2400$; the Prandtl and Schmidt numbers $Pr = 1$ and $Sc = 1$ respectively; and the nondimensional heating rate which is quantified, as in earlier studies (Bhat & Narasimha, 1996; Aspden *et al.*, 2017), using the “heat-release number” (or the bulk Richardson number)

$$G = \left[\frac{g\beta_T \alpha_C d^2}{U_o^3} \right] \left[\frac{dU_o^3}{b_b U_b^3} \right] \frac{1}{d^3} \int_{z_b}^{z_t} \int_0^\infty 2\pi r \bar{C} dr dz, \quad (2)$$

which is the ratio of total buoyancy added in the HIZ to flow inertia at z_b , with the overbar in $\bar{C}(r, z)$ denoting temporal and azimuthal averaging. This quantity is an output from the dynamics, and must be determined *a posteriori*. The value for

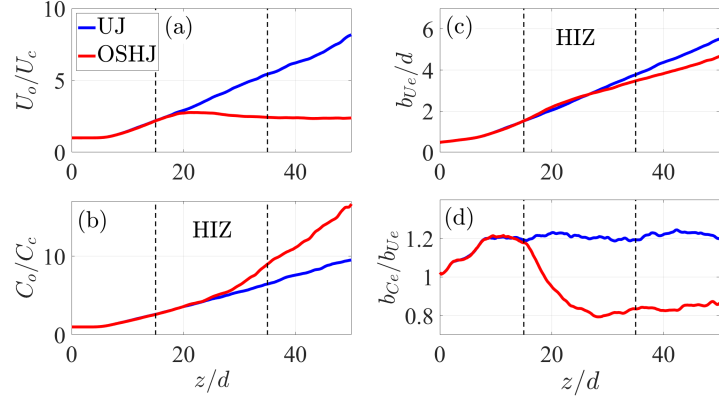


Figure 2. Axial variation of (a) the centerline velocity U_c , (b) centerline passive scalar concentration C_c (c) the $1/e$ width of velocity profile b_{U_e} , and (d) the ratio of scalar to velocity flow widths $\xi_C = b_{C_e}/b_{U_e}$ for heated and unheated jets. The dashed lines represent the extent of the HIZ.

$G = 0.37$, is obtained with a pre-set parameter $g\beta_T \alpha_C d^2/U_o^3 (= 0.0008)$ for the simulation reported here, is comparable to those in earlier studies (see Table 1).

The equations (1) are solved using the finite volume solver *Megha-5*, which has been extensively used and validated, including in simulations of unheated jet & plume in Singhal *et al.* (2021) and dry & moist thermals in Vybhav & Ravichandran (2021). The boundary conditions and other numerical details are similar to those used in Singhal *et al.* (2021) for a canonical jet, except that heat is added externally. We compare the heated jet with the unheated jet obtained by setting $\alpha_C = 0$ in equations (1). Hereinafter, we refer to the canonical round turbulent jet as the “unheated jet” (UJ), and the flows with heat added externally that we study here as “off-source heated jets” (OSHJ). We report results of the UJ and OSHJ averaged over 1440 and 1120 flow units respectively, which are sufficiently long for the statistics to converge (see figures 2, 8, 9, 10 and 11). Averages are performed over a smaller time interval in the OSHJ since the local eddy-turnover times ($\propto b_{ue}/U_c$) are smaller for this case.

The axial variation of the characteristic scales in unheated and heated jets is shown in figure 2. The decay rate of the centerline velocity U_c , and the spread rate of the width (b_{ue} , defined as $\bar{u}(z, r = b_{ue}) = U_c(z)/e$) are found to be 6.18 and 0.114 respectively for UJ and lie within the range observed in Panchapakesan & Lumley (1993). Similarly, for UJ, the centerline scalar concentration C_c decays as $C_c \sim 1/z$, with the ratio of scalar to velocity widths $\xi_C = b_{C_e}/b_{ue} \approx 1.21$, in agreement with Turner (1986); Kaminski *et al.* (2005). These results act as further validation of the numerical methods employed here. In the OSHJ, we see (i) a slower decay or mild increase of $U_c(z)$, (ii) jet width undergo an initial increase followed by a low spread rate compared to UJ, (iii) a faster decay of $C_c(z)$, and (iv) a smaller value ξ_C relative to the UJ. In both the UJ and the OSHJ, we find that the radial profiles of the temporally and azimuthally averaged velocity and scalar concentration are Gaussian (see figure 8), in agreement with earlier studies, whereas the radial profiles of the temperature are *not* Gaussian in beginning of HIZ.

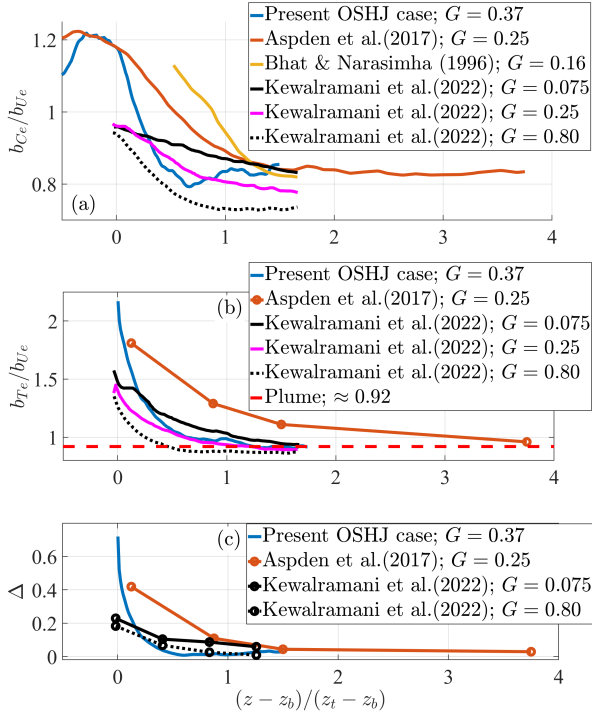


Figure 3. (a) The ratio of scalar to velocity flow widths ξ_C (see text for explanation). (b) The ratio of temperature to velocity flow widths, ξ_T . (c) The deviation Δ of the temperature profile from the self-similar Gaussian profile. The horizontal axis in each graph is the scaled axial length in which $0 < \bar{z} < 1$ is the heat-injection zone.

RESULTS AND DISCUSSION

A prominent feature of heated jets is the reduction of the growth rate of the scalar flow-width b_{Ce} . We observe, in agreement with earlier studies, that off-source heat addition leads to a reduction in the ratio ξ_C . In figure 3(a), we plot the variation of ξ_C with the scaled axial distance $\bar{z} = (z - z_b)/(z_t - z_b)$. In agreement with previous studies (except Kewalramani *et al.* (2022)), we see that $\xi_C \approx 1.2$ for $\bar{z} < 0$, and rapidly drops to $\xi_C \approx 0.83$ at $\bar{z} \approx 0.5$. We see by comparing the data from Bhat & Narasimha (1996) and Aspden *et al.* (2017) with the present OSHJ (figure 3(a)) that the final value of the width ratio attained is $\xi_C \approx 0.83$. The location z_b of the base of the HIZ, its extent, and the amount of heat added are quite different in these studies (see Table 1). In view of this, the observation that approximately the same value of $\xi_C \approx 0.83$ is realised after heat addition is interesting, although its cause is not immediately clear. We may also infer that for larger heating rates (larger G), the scaled distance at which ξ_C reaches its final value decreases. Thus, in Aspden *et al.* (2017) & Bhat & Narasimha (1996), the value $\xi_C \approx 0.83$ is attained above the HIZ ($z > z_t$). In contrast, in the present OSHJ study, we see that ξ_C briefly decreases to a lower value before reaching its final value at $\bar{z} \approx 0.5$. We also note that the numerical value $\xi_C = 0.83$ is approximately the inverse of the value $\xi_{C,UJ} \approx 1.21$ in UJs. For the LES of Kewalramani *et al.* (2022), for $G = 0.075$, $\xi_C \approx 0.83$ is realized for $\bar{z} > 1$ but for the higher heating rates ξ_C reaches a value less than 0.8 (figure 3(a)). It is worth noting that for Kewalramani *et al.* (2022), $\xi_C < 1$ for $\bar{z} = 0$ which is a somewhat unexpected behaviour.

The analogous ratio $\xi_T = b_{Te}/b_{Ue}$ for the temperature is plotted in figure 3(b), and compared against data from Aspden *et al.* (2017) and Kewalramani *et al.* (2022). Again, we see that

the ratio ξ_T rapidly decreases upon heat addition, attaining a final value $\xi_T \approx 0.92 < 1$. Note that this value falls within the range $\xi_T \in [0.88, 1.07]$, typically found in the self-similar region of a (classical) plume (Kaminski *et al.*, 2005). Interestingly, the behaviour of ξ_T for Kewalramani *et al.* (2022) matches well with that for others unlike that of ξ_C . While ξ_C and ξ_T quantities are available in Agrawal *et al.* (2005) (see their figure 8), they are not plotted here in figure 3. This is due to very large heating number, $G = 12$ (denoted as Ri_* in Agrawal *et al.* (2005)), which makes it difficult to directly compare their results with those of others.

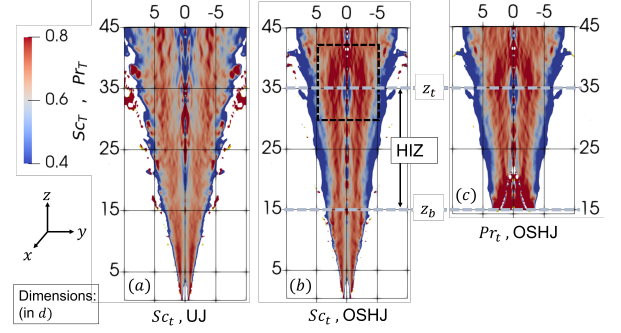


Figure 4. (a) The turbulent Schmidt number Sc_t in the UJ, and (b, c) Sc_t and the turbulent Prandtl number Pr_t in the OSHJ on a vertical plane containing the flow axis.

The profiles of \bar{T} peak away from the jet centerline at the beginning of the HIZ (shown in figure 8(c), and also seen in Aspden *et al.* (2017); Kewalramani *et al.* (2022)). In figure 3(c), we quantify the RMS deviation Δ from the self-similar Gaussian profile, showing that the OSHJ becomes self-similar (in its first-order statistics) for $\bar{z} > \bar{z}_{ss} \approx 0.5$ (subscript “ss” for self-similar). We again see that \bar{z}_{ss} tends to decrease as G increases. From figures 3(a-c), we see that the width ratios $\xi_{C,T}$ reach their steady post-HIZ values nearly at the same axial location where the temperature profiles become Gaussian and self-similar. Thus \bar{z}_{ss} represents the location of onset of another regime of self-similar behaviour after heat addition, especially with regard to the scalar and temperature distributions. We also see that while some properties of the OSHJ, such as the ratio ξ_T (here) and the entrainment coefficient (Aspden *et al.*, 2017) are similar to those of a classical plume, other features such as the turbulent Prandtl number Pr_t are distinct from those in a classical plume (as discussed below).

The turbulent transport of scalar concentration and temperature are quantified using the Schmidt and Prandtl numbers, $Sc_t = \nu_t/D_t$, and $Pr_t = \nu_t/\alpha_t$, where ν_t , D_t and α_t are the turbulent diffusivities of axial momentum, scalar concentration and temperature:

$$\nu_t = -\frac{\overline{u_r u_z}}{\partial \overline{u_z} / \partial r} ; D_t = -\frac{\overline{u_r C'}}{\partial \overline{C} / \partial r} ; \alpha_t = -\frac{\overline{u_r T'}}{\partial \overline{T} / \partial r} . \quad (3)$$

The correlations of fluctuating quantities in equation (3) are averaged temporally and azimuthally, and their normalized radial variations plotted later in figure 9, 10 and 11, respectively. The effect of off-source heating on the Sc_t is shown in figure 4, where we see that Sc_t for the OSHJ is larger than that for the UJ in the core of the jet for $z \gtrsim z_t$, and decays more rapidly with the radius for $r \gtrsim b_{Ue}$. Thus in comparison

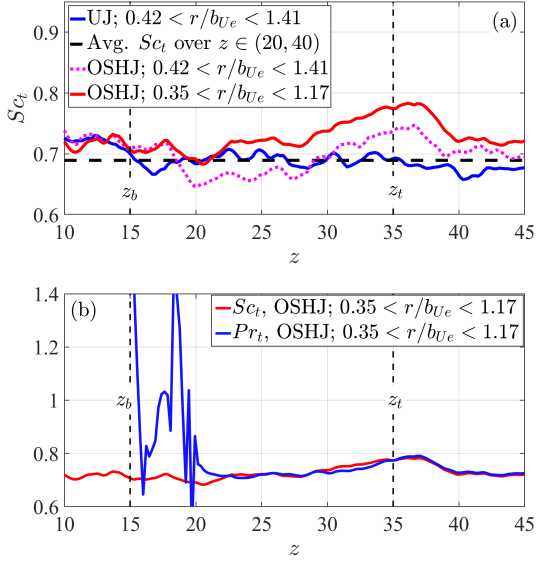


Figure 5. (a) Sc_t for the UJ and OSHJ. In the OSHJ, the radial averages are also performed over a smaller radial extent since we know from figure 4 that the scalar flow-width is smaller (b) Pr_t and Sc_t in the OSHJ.

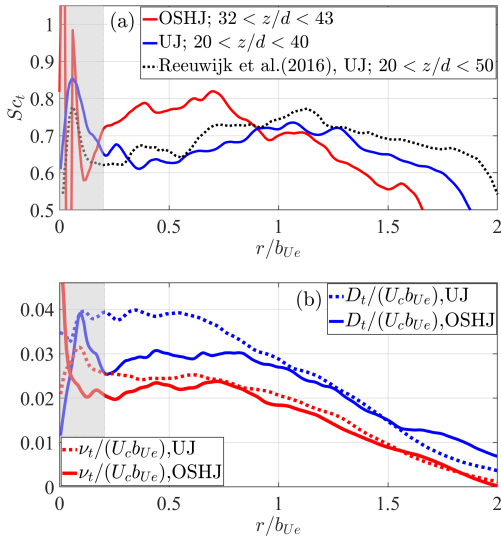


Figure 6. (a) The radial variation of the turbulent Schmidt number in the self-similar region of the UJ and the post-HIZ region ($32d - 43d$) in the OSHJ. (b) The turbulent diffusivity of axial velocity (v_t) and scalar (D_t) for the UJ and OSHJ. In both (a) and (b), azimuthal averages of D_t , v_t and Sc_t are unreliable in the shaded region ($r/b_{Ue} < 0.2$) near the jet's axis.

with UJ, heat addition in OSHJ produces two different regions with a large difference in Sc_t (see also figure 6(a)). The region close to axis with higher Sc_t , the ‘core’, could have qualitatively different features with respect to the region near edge as suggested in the Bhat & Narasimha (1996). They also observed an enhanced mixing within the core of the heated jet. The implications of our results towards this observation is a topic of future work.

We plot the axial profiles of the radially and temporally averaged Sc_t for the unheated and heated jet in figure 5(a). For UJ, we find that Sc_t has an average value of 0.69 over

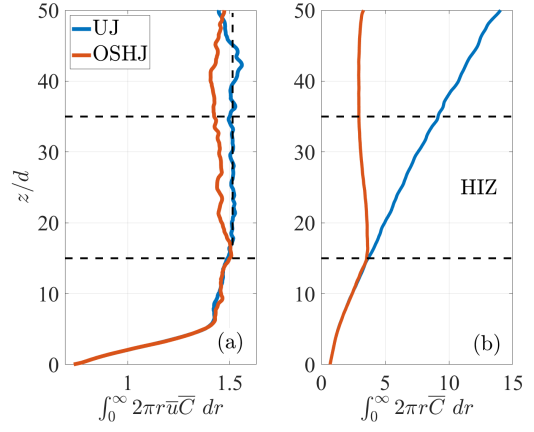


Figure 7. (a) Total scalar flux and (b) total scalar present at different locations in unheated and off-source heated jet.

$z \in (20, 40)$ and $r/b_{Ue} \in (0.42, 1.41)$, comparable with the value of 0.72 found by Reeuwijk *et al.* (2016). The radial range $0.42 < r/b_{Ue} < 1.41$, however, does not capture the behaviour of Sc_t for $z \gtrsim z_t$ seen in figure 4(b). We therefore average over a narrower radial range $0.35 < r/b_{Ue} < 1.17$, obtained by multiplying the earlier range by a factor of $\xi_C = 0.83$. This curve, also shown in figure 5(b), better reflects the behaviour seen in figure 4(b). Next, we plot Pr_t for the OSHJ in figure 5(b), where we find that Pr_t takes on large values for $z \approx z_b$ before reaching a steady value approximately equal to the value of Sc_t . This value, $Pr_t > 0.75$ near $z \approx z_t$, is larger than the range of values $Pr_{t, plume} \in (0.62, 0.67)$ found in steady turbulent plumes (Wang & Law, 2002; Reeuwijk *et al.*, 2016), although the ratio ξ_T of temperature to velocity widths is similar in OSHJs and plumes, as seen earlier (figure 3b).

The radial profiles of the azimuthally, axially and temporally averaged Sc_t for the OSHJ are compared with the Sc_t for a UJ in figure 6(a). The large deviations close to the axis (the grey semi-transparent region; $r/b_{Ue} < 0.2$) are due to the smaller number of grid points available and due to the small numerical values of the radial derivative $\partial/\partial r$. For $r/b_{Ue} > 0.2$, the variations are smoother; the small wiggles observed, which are also seen for the curve of Reeuwijk *et al.* (2016), are due to the sensitive dependence of $\partial \bar{C}/\partial r$ on the precise radial variation of \bar{C} and not due to inadequate statistical averaging. The averages in the OSHJ are performed over an axial range $32d < z < 43d$ where the Sc_t in the core of OSHJ is largest (see figure 4). We find that, in the interval $0.2 < r/b_{Ue} \lesssim 0.8$, Sc_t is larger for the OSHJ than for the UJ. We also see a steeper decrease in Sc_t in the OSHJ away from the axis. To examine why Sc_t is larger in the OSHJ, we have plotted normalized v_t and D_t separately in figure 6(b), showing that heat addition reduces D_t of the scalar in the region $r/b_{Ue} \lesssim 0.8$, while v_t is much less affected. The lower value of D_t is responsible for the reduction of ξ_C in the OSHJ. Evidently, the larger turbulent radial flux $\bar{u}_r \bar{C}$ in the OSHJ (see figure 10(b)), is offset by the large gradient $\partial \bar{C}/\partial r$.

Lastly, we discuss total scalar flux and total scalar mass ($m_c(z)$) per unit axial distance available at different z locations, quantified using the Gaussian profile parameters

$$\int_0^\infty 2\pi r \bar{u} \bar{C} dr = 2\pi C_c U_c \frac{b_{C_e}^2 b_{U_e}^2}{b_{C_e}^2 + b_{U_e}^2} = 2\pi C_c U_c b_{U_e}^2 \frac{\xi_C^2}{\xi_C^2 + 1};$$

$$\text{and } m_c(z) = \int_0^\infty 2\pi r \bar{C} dr = \pi C_c b_{C_e}^2 = \pi C_c b_{U_e}^2 \xi_C^2. \quad (4)$$

In the fully developed unheated jet, the total scalar flux is axially invariant and the total scalar mass increases linearly with axial distance, as expected from the relations $U_c, C_c \propto 1/z$ & $b_e \propto z$, and shown in figure 7. The external addition of heat changes these profiles. From the radial balance of scalar concentration, which reads

$$\frac{d}{dz} \left[\int_0^\infty r \bar{u} \bar{C} dr \right] + \frac{d}{dz} \left[\int_0^\infty r \bar{u}'_z \bar{C}' dr \right] = 0. \quad (5)$$

we see that the behaviour of the turbulent scalar flux $\bar{u}'_z \bar{C}'$ determines the profile of the mean scalar flux. Heat addition leads to positive values of $\partial \bar{u}'_z \bar{C}' / \partial z$ in the HIZ (see figure 10), and thus a reduction in the scalar flux (see figure 7(a)), as well as ξ_C (figure 3(b)). The total scalar mass $m_C(z)$ in the OSHJ is constant with axial distance, despite the increase of the mass flow rate ($m_u(z) = \int_0^\infty 2\pi r \bar{u} dr$) (see Bhat & Narasimha (1996); Aspden *et al.* (2017)); the decaying centreline scalar concentration and increasing b_{C_e} (figure 2) evidently offset each other. The relationship between the entrainment and the scalar dilution in an OSHJ can have direct implications for cumulus cloud flows. The connection of the statistical behaviour reported here with the coherent motions in the off-source heated jet is another fruitful line of investigation worth pursuing.

CONCLUSION

In summary, our DNS results suggest that the OSHJ attains a nearly self-similar state, some distance above z_b , in the core of which the turbulent Schmid number Sc_t is larger, and for which the ratio ξ_C lower, than in an unheated jet. The turbulent Prandtl number Pr_t in this self-similar heated jet is also larger, but does not seem to lead to a concomitant decrease in the ratio ξ_T beyond the heating zone. The flow thus has a core-annular structure, with Pr_t and Sc_t attaining greater values, and decaying more rapidly with radius, than in an unheated jet. We also found that the linear growth in the total passive scalar content with axial distance is arrested by heat addition. These differences and their possible implications for cumulus cloud dynamics make the off-source heated jet a valuable model for future study.

S.S.D. acknowledges support from IISc Bengaluru towards running the simulations at its supercomputing facility. S.R. is supported under Swedish Research Council grant no. 638-2013-9243. We thank the reviewers for their useful comments.

REFERENCES

- Agrawal, A, Boersma, B-J & Prasad, A K 2005 Direct numerical simulation of a turbulent axisymmetric jet with buoyancy induced acceleration. *Flow, turbulence and combustion* **73** (3-4), 277–305.
- Agrawal, A & Prasad, A K 2004 Evolution of a turbulent jet subjected to volumetric heating. *J. Fluid Mech.* **511**, 95–123.
- Aspden, AJ, Nikiforakis, N, Bell, JB & Dalziel, S B 2017 Turbulent jets with off-source heating. *J. Fluid Mech.* **824**, 766–784.
- Bhat, GS & Narasimha, R 1996 A volumetrically heated jet: large-eddy structure and entrainment characteristics. *J. Fluid Mech.* **325**, 303–330.
- Kaminski, E, Tait, S & Carazzo, G 2005 Turbulent entrainment in jets with arbitrary buoyancy. *J. Fluid Mech.* **526**, 361–376.

- Kewalramani, G, Pant, C S & Bhattacharya, A 2022 Energy consistent gaussian integral model for jet with off-source heating. *Phys. Rev. Fluids* **7** (1), 013801.
- Narasimha, R, Diwan, S S, Duvvuri, S, Sreenivas, KR & Bhat, GS 2011 Laboratory simulations show diabatic heating drives cumulus-cloud evolution and entrainment. *PNAS* **108** (39), 16164–16169.
- Panchapakesan, N R & Lumley, J L 1993 Turbulence measurements in axisymmetric jets of air and helium. part 1. air jet. *J. Fluid Mech.* **246**, 197–223.
- Reeuwijk, M V, Salizzoni, P, Hunt, G R & Craske, J 2016 Turbulent transport and entrainment in jets and plumes: a dns study. *Phys. Rev. Fluids* **1** (7), 074301.
- Singhal, R, Ravichandran, S, Diwan, S S & Brown, G L 2021 Reynolds Stress Gradient and Vorticity Fluxes in Axisymmetric Turbulent Jet and Plume. In *Proceedings of 16th Asian Congress of Fluid Mech.* (ed. L. Venkatakrishnan *et al.*). Bangalore.
- Turner, J S 1986 Turbulent entrainment: the development of the entrainment assumption, and its application to geophysical flows. *J. Fluid Mech.* **173**, 431–471.
- Venkatakrishnan, L 1997 Development of a plume with off-source volumetric heating. PhD thesis.
- Vybhav, GR & Ravichandran, S 2021 Entrainment in dry and moist thermals. *Phys. Rev. Fluids* (in press).
- Wang, H & Law, A W 2002 Second-order integral model for a round turbulent buoyant jet. *J. Fluid Mech.* **459**, 397–428.

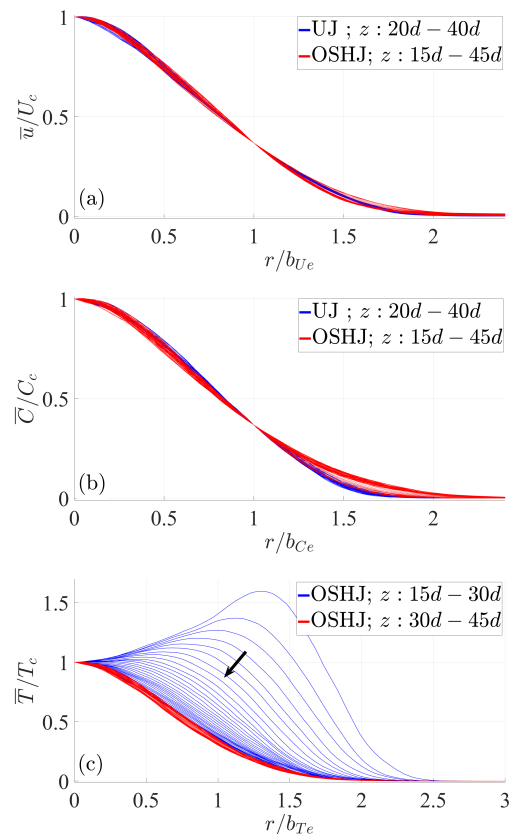


Figure 8. Radial profile of first order statistics of field variables: (a) axial velocity (\bar{u}), (b) scalar concentration (\bar{C}), and (c) Temperature (\bar{T}). The arrow sign in (c) represents the evolution of temperature profile with respect to downstream axial direction.

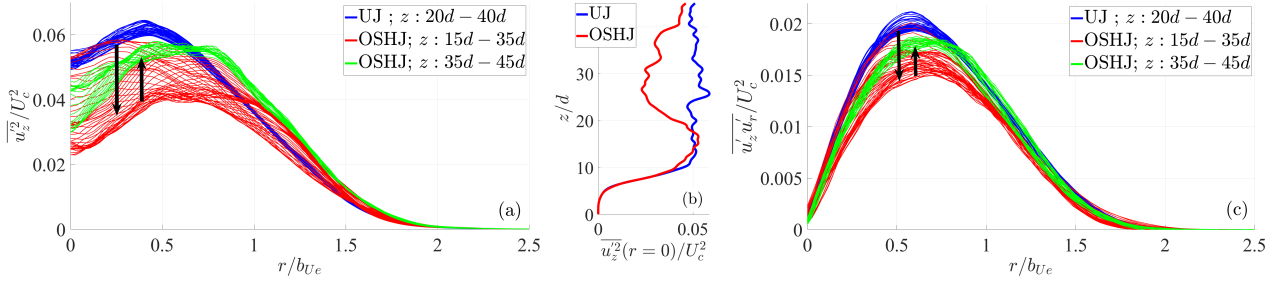


Figure 9. (a) Radial profiles of $\overline{u_z^2}$ (b) axial variation of center-line axial turbulent intensity $\overline{u_z^2}$, and (c) radial profiles of $\overline{u_z u_r}$ in unheated and off-source heated jet. In OSHJ case, we see decrement in velocity correlations with a later recovery in axial distance; direction of increment or decrement is shown by arrows.

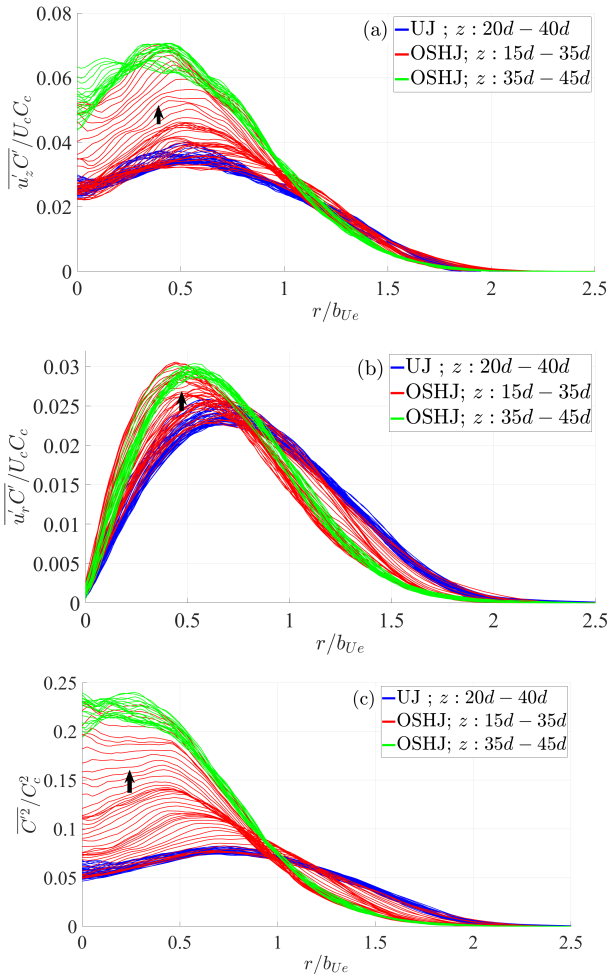


Figure 10. Radial self-similar profiles of second-order quantities (a) $\overline{u_z C'}$, (b) $\overline{u_r C'}$ and (c) $\overline{C'^2}$ in unheated and off-source heated jet. Unheated jet shows collapse of all the profile to a self-similar curve. In OSHJ case, we can see an increase in velocity scalar correlation with increase in axial distance after starting of HIZ; direction of increase is shown by arrow on red curves.

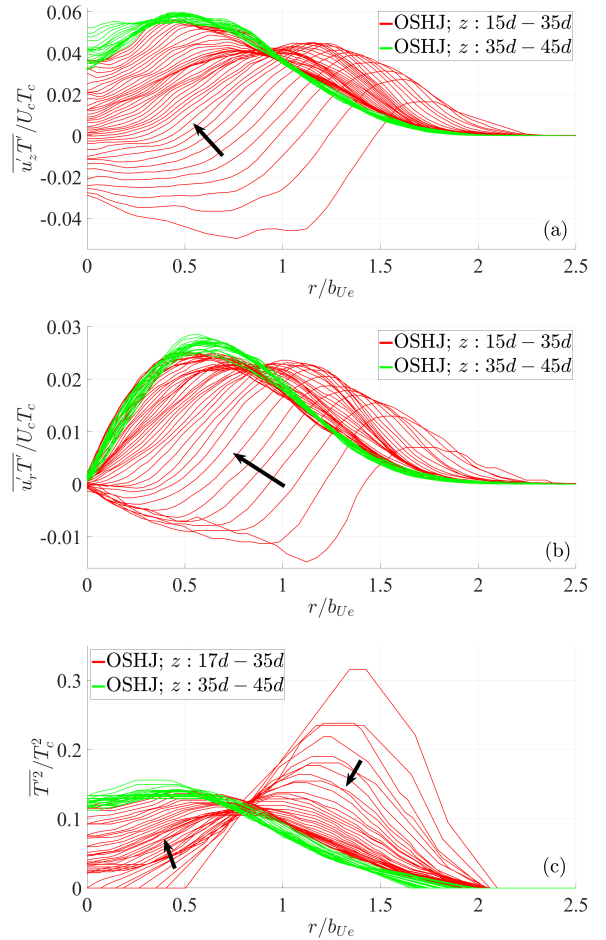


Figure 11. Radial self-similar profiles of second-order quantities (a) $\overline{u_z T'}$, (b) $\overline{u_r T'}$ and (c) $\overline{T'^2}$ in unheated and off-source heated jet. The arrow sign represents the evolution of profiles with respect to downstream axial direction. Here, the negative correlation signifies that low velocity regions undergo a higher heating (hence, temperature).